

Current-induced dynamics in non-collinear dual spin-valves

P. Baláz^{1,*} M. Gmitra² and J. Barnaś^{1,3}

¹*Department of Physics, Adam Mickiewicz University, Umultowska 85, 61-614 Poznań, Poland*

²*Institute of Phys., P. J. Šafárik University, Park Angelinum 9, 040 01 Košice, Slovak Republic*

³*Institute of Molecular Physics, Polish Academy of Sciences Smoluchowskiego 17, 60-179 Poznań, Poland*

(Dated: October 22, 2018)

Spin-transfer torque and current induced spin dynamics in spin-valve nanopillars with the free magnetic layer located between two magnetic films of fixed magnetic moments is considered theoretically. The spin-transfer torque in the limit of diffusive spin transport is calculated as a function of magnetic configuration. It is shown that non-collinear magnetic configuration of the outermost magnetic layers has a strong influence on the spin torque and spin dynamics of the central free layer. Employing macrospin simulations we make some predictions on the free layer spin dynamics in spin valves composed of various magnetic layers. We also present a formula for critical current in non-collinear magnetic configurations, which shows that the magnitude of critical current can be several times smaller than that in typical single spin valves.

PACS numbers:

I. INTRODUCTION

Magnetic multilayers are ones of the most relevant elements in the development of cutting-edge technologies. If current flows along the axis of a metallic hybrid nanopillar structure, a spin accumulation builds up in the vicinity of the normal-metal/ferromagnet interface. Moreover, the current produces spin-transfer torque (STT) which acts on magnetic moments of the ferromagnetic layers^{1,2}. As a consequence, magnetization of a particular layer may be driven to an oscillation mode³, or can be switched between possible stable states⁴. However, current-induced control of magnetic moments requires a rather high current density. Therefore, reduction of the critical current density remains the most challenging requirement from the point of view of possible applications. Since the critical currents are related to STT, which in the diffusive transport regime is proportional to spin accumulation at the normal-metal/ferromagnet interface, one may alternatively rise a question of possible ways to enhance the spin accumulation.

One of the possibilities to decrease the critical current density in metallic structures is the geometry proposed by L. Berger⁵, in which the free magnetic layer is located between two pinned magnetic layers of opposite magnetizations. Indeed, in such a *dual spin valve* (DSV) geometry both interfaces of the free layer can generate STT, and this may decrease the critical current several times⁵.

To examine the influence of an additional magnetic layer on the free layer's spin dynamics one needs to find first the STT acting on the central layer for arbitrary direction of its magnetization vector. To do this, we employ the spin-dependent diffusive transport approach⁶, based on Valet-Fert description⁷. In this paper we present a comprehensive survey of STT-induced effects in DSVs for generally non-collinear magnetic configuration of the outermost magnetic films. We also study asymmetric exchange-biased DSV, in which magnetic moment of one of the outer magnetic layers is fixed to an antiferromag-

netic layer due to exchange anisotropy. We show that a non-standard (wavy-like) angular dependence of STT – originally predicted for asymmetric spin valves^{6,8} – can also occur in DSV geometry. Such a non-standard angular dependence of the torque is of some importance from the application point of view, as it allows to induce steady-state precessional modes without external magnetic field^{8,10}. Furthermore, we examine current-induced spin dynamics within the macrospin model, and derive a formula for critical currents which destabilize trivial fixed points of the central spin's dynamics in non-collinear configurations of the outermost magnetizations.

In section II we describe the model and introduce basic formula for STT and spin dynamics in DSVs. Then, in section III we study dynamics in a symmetric DSV geometry, where we compare STT and spin dynamics in DSVs and single spin valves (SSVs). Finally, in section IV we analyze an exchange-biased DSV structure with noncollinear magnetic moments of the outermost magnetic layers. Finally, we conclude in section V.

II. MODEL

We consider a multilayer nanopillar structure, $F_L/N_L/F_C/N_R/F_R$, consisting of three ferromagnetic (F) layers separated by normal-metal (N) layers; see Fig. 1. Spin moment of the central layer, F_C , is free to rotate, while the right F_R and left F_L ferromagnetic layers are much thicker and their net spin moments are assumed to be fixed for current densities of interest. Fixing of these moments can be achieved either by sufficiently strong coercive fields, or by exchange anisotropy at interfaces with antiferromagnetic materials.

In the Landau-Lifshitz-Gilbert phenomenological description, the dynamics of a unit vector along the net spin moment \hat{s} of the central (free) magnetic layer is de-

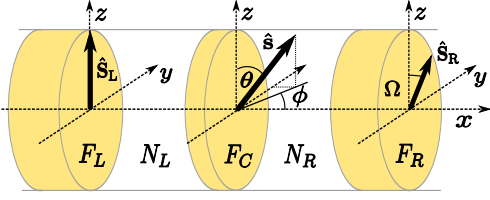


FIG. 1: Schematic of a dual spin valve with fixed magnetic moments of the outer magnetic layers, F_L and F_R , and free central magnetic layer, F_C , separated by normal-metal layers N_L and N_R . Here, \hat{S}_L , \hat{S}_R , and \hat{s} are unit vectors along the spin moments of the F_L , F_R , and F_C layers, respectively.

scribed by the equation

$$\frac{d\hat{s}}{dt} + \alpha \hat{s} \times \frac{d\hat{s}}{dt} = \Gamma, \quad (1)$$

where α is the Gilbert damping parameter. The right-hand side represents the torques due to effective magnetic field and spin-transfer,

$$\Gamma = -|\gamma_g| \mu_0 \hat{s} \times \mathbf{H}_{\text{eff}} + \frac{|\gamma_g|}{M_s d} \boldsymbol{\tau}, \quad (2)$$

where γ_g is the gyromagnetic ratio, μ_0 is the vacuum permeability, M_s stands for the saturation magnetization of the free layer, and d denotes thickness of the free layer. Considering the thin ferromagnetic free layer of elliptical cross-section, the effective magnetic field \mathbf{H}_{eff} can be written as

$$\mathbf{H}_{\text{eff}} = -H_{\text{ext}} \hat{e}_z - H_{\text{ani}} (\hat{s} \cdot \hat{e}_z) \hat{e}_z + \mathbf{H}_{\text{dem}}, \quad (3)$$

and includes applied external magnetic field (H_{ext}), uniaxial anisotropy field (H_{ani}), and the demagnetization field (\mathbf{H}_{dem}), where \hat{e}_z is the unit vector along the z -axis (easy axis), compare scheme in Fig. 1. The demagnetization field can be written in the form $\mathbf{H}_{\text{dem}} = (\hat{s} \cdot \bar{\mathbf{N}}) M_s = (H_{dx} s_x, H_{dy} s_y, H_{dz} s_z)$, where $\bar{\mathbf{N}}$ is a diagonal demagnetization tensor.

Spin-transfer torque

Generally, STT acting on a magnetic layer is determined by the electron spin angular momentum absorbed

from conduction electrons within a few interfacial atomic layers of the ferromagnet¹¹. Thus, the STT acting on the central layer F_C can be calculated as $\boldsymbol{\tau} = (\hbar/2) (\mathbf{j}_{\perp}^L - \mathbf{j}_{\perp}^R)$, where \mathbf{j}_{\perp}^L and \mathbf{j}_{\perp}^R are the spin current components perpendicular to magnetic moment of the free layer and calculated at the corresponding left and right normal-metal/ferromagnet interfaces. The torque consists of in-plane $\boldsymbol{\tau}_{\parallel}$ (in the plane formed by magnetic moments of the two interacting films) and out-of-plane $\boldsymbol{\tau}_{\perp}$ (normal to this plane) parts, $\boldsymbol{\tau} = \boldsymbol{\tau}_{\parallel} + \boldsymbol{\tau}_{\perp}$, which have the following forms

$$\boldsymbol{\tau}_{\parallel} = I \hat{s} \times \left[\hat{s} \times (a_L \hat{S}_L - a_R \hat{S}_R) \right], \quad (4a)$$

$$\boldsymbol{\tau}_{\perp} = I \hat{s} \times (b_L \hat{S}_L - b_R \hat{S}_R), \quad (4b)$$

where I is the current density, and \hat{S}_L and \hat{S}_R are the unit vectors pointing along the fixed net-spins of the F_L and F_R layers, respectively. The parameters a_L , a_R , b_L , and b_R depend, generally, on the magnetic configuration and material composition of the system, and have been calculated in the diffusive transport limit⁶. According to first-principles calculations of the mixing conductance¹², the out-of-plane torque in metallic structures is about two orders of magnitude smaller than the in-plane torque. Although this component has a minor influence on critical currents, it may influence dynamical regimes, so we include it for completeness in our numerical calculations.

Let us consider now how the STT affects spin dynamics of the free magnetic layer. We rewrite Eq.(1) in spherical coordinates (ϕ, θ) , which obey $\hat{s} = (\cos \phi \sin \theta, \sin \phi \sin \theta, \cos \theta)$; see Fig. 1. Defining unit base vectors, $\hat{e}_{\phi} = (\hat{e}_z \times \hat{s}) / \sin \theta$ and $\hat{e}_{\theta} = \hat{e}_{\phi} \times \hat{s}$, Eq.(1) can be rewritten as

$$\frac{d}{dt} \begin{pmatrix} \phi \\ \theta \end{pmatrix} = \frac{1}{1 + \alpha^2} \begin{pmatrix} \sin^{-1} \theta & -\alpha \sin^{-1} \theta \\ \alpha & 1 \end{pmatrix} \begin{pmatrix} v_{\phi} \\ v_{\theta} \end{pmatrix}, \quad (5)$$

where the overall torques v_{θ} and v_{ϕ} , changing the angles θ and ϕ , respectively, read

$$v_{\theta} = \Gamma \cdot \hat{e}_{\theta} = -|\gamma_g| \mu_0 (H_{dx} - H_{dy}) \cos \phi \sin \phi \sin \theta + \frac{|\gamma_g|}{M_s d} \tau_{\theta}, \quad (6a)$$

$$v_{\phi} = \Gamma \cdot \hat{e}_{\phi} = -|\gamma_g| \mu_0 [H_{\text{ext}} + (H_{\text{ani}} + H_{dx} \cos^2 \phi + H_{dy} \sin^2 \phi - H_{dz}) \cos \theta] \sin \theta + \frac{|\gamma_g|}{M_s d} \tau_{\phi}. \quad (6b)$$

The first terms in Eqs. (6) describe the torques due to

demagnetization and anisotropy fields of the free layer,

while $\tau_\theta = \tau_\theta^\parallel + \tau_\theta^\perp$ and $\tau_\phi = \tau_\phi^\parallel + \tau_\phi^\perp$ are the corresponding components of the current-induced torque, which originate from τ_\parallel and τ_\perp .

As we have already mentioned above, the main contribution to STT comes from τ_\parallel . Assuming now that magnetic moment of the left magnetic layer is fixed along the z -axis, $\hat{\mathbf{S}}_L = (0, 0, 1)$, and magnetic moment of the right magnetic layer is rotated by an angle Ω from the z -axis and fixed in the layer's plane (see Fig. 1), $\hat{\mathbf{S}}_R = (0, \sin \Omega, \cos \Omega)$, one finds

$$\tau_\theta^\parallel = (a_L - a_R \cos \Omega) I \sin \theta + a_R I \sin \Omega \sin \phi \cos \theta, \quad (7a)$$

$$\tau_\phi^\parallel = a_R I \cos \phi \sin \Omega. \quad (7b)$$

The component τ_θ^\parallel consists of two terms. The first one is analogous to the term which describes STT in a SSV. However, its amplitude is now modulated due to the presence of F_R . In turn, the second term in Eq. (7a) is nonzero only in noncollinear magnetic configurations. From Eq. (7b) follows that τ_ϕ^\parallel is also nonzero in noncollinear configurations, and only if the magnetization points out of the layer's plane ($\phi \neq \pi/2$). When magnetic moments of the outer magnetic layers are parallel ($\Omega = 0$), $\tau_\theta^\parallel = (a_L - a_R) I \sin \theta$. For a symmetric DSV, $a_L(\theta) = a_R(\theta)$, and hence STT acting on $\hat{\mathbf{s}}$ vanishes. On the other hand, in the antiparallel configuration of $\hat{\mathbf{S}}_L$ and $\hat{\mathbf{S}}_R$ ($\Omega = \pi$), the maximal spin torque enhancement can be achieved, $\tau_\theta^\parallel = (a_L + a_R) I \sin \theta$.

Similar analysis of τ_\perp leads to the following formulas for τ_θ^\perp and τ_ϕ^\perp :

$$\tau_\theta^\perp = b_R I \cos \phi \sin \Omega, \quad (8a)$$

$$\tau_\phi^\perp = -(b_L - b_R \cos \Omega) I \sin \theta + b_R \cos \theta \sin \phi \sin \Omega. \quad (8b)$$

Thus, if the outer magnetic moments are collinear, $\tau_\theta^\perp = 0$, while τ_ϕ^\perp reduces to $\tau_\phi^\perp = -(b_L - b_R) I \sin \theta$ for $\Omega = 0$, and $\tau_\phi^\perp = -(b_L + b_R) I \sin \theta$ for $\Omega = \pi$. Hence, in symmetric spin valves, where $b_L = b_R$, τ_ϕ^\perp vanishes in the parallel configuration of the outermost magnetic moments and is enhanced in the antiparallel configuration.

In the following sections we investigate STT and its effects on critical current and spin dynamics. We start from symmetric spin valves in antiparallel magnetic configuration ($\Omega = \pi$). Then, we proceed with asymmetric exchange-biased dual spin valves.

III. SYMMETRIC DSVS

Let us consider first symmetric DSVs with antiparallel orientation of magnetic moments of the outermost ferromagnetic films: $\hat{\mathbf{S}}_L = (0, 0, 1)$ and $\hat{\mathbf{S}}_R = (0, 0, -1)$. As indicated by Eqs. (7) and (8), such a configuration may lead to enhancement of STT in comparison to that in SSVs. Thus, let us analyze first STT in two types of structures: the double spin valve F(20)/Cu(10)/F(8)/Cu(10)/F(20)

in the antiparallel configuration, and the corresponding single spin valve F(20)/Cu(10)/F(8). The numbers in brackets correspond to layer thicknesses in nanometers.

In Fig. 2 we show the angular dependence of STT for DSVs and SSVs, when the vector $\hat{\mathbf{s}}$ changes its orientation, described by angle θ , in the layer plane ($\phi = \pi/2$). The magnetic layers made of Permalloy, Ni₈₀Fe₂₀ (Fig. 2a), and of Cobalt (Fig. 2b) are considered. Due to the additional fixed layer (F_R), STT in DSVs is about twice as large as in SSVs, which is consistent with Berger's predictions². Additionally, the angular dependence of STT acting on the free layer in Co/Cu/Co spin valves is more asymmetric than in Py/Cu/Py. This asymmetry, however, disappears in Co/Cu/Co/Cu/Co DSVs due to superposition of the contributions from both fixed magnetic layers to the STT.

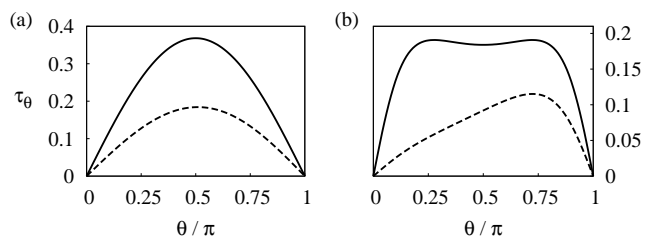


FIG. 2: Spin transfer torque τ_θ in symmetric DSVs, F(20)/Cu(10)/F(8)/Cu(10)/F(20), in the antiparallel configuration, $\Omega = \pi$, (solid lines), and STT in SSVs, F(20)/Cu(10)/F(8) (dashed lines), where (a) F = Permalloy, (b) F = Cobalt. STT is shown in the units of $\hbar|I|/|e|$, and calculated for $\phi = \pi/2$. The material parameters as in Ref.13.

The enhancement of STT in dual spin valves may lead to two important improvements of the spin dynamics: reduction of the critical current needed to trigger the spin dynamics, and decrease of the switching time. The latter is defined as the time needed to switch the magnetization from one stable position to the opposite one. The fixed points of the dynamics of $\hat{\mathbf{s}}$ are given by the equations $v_\theta = 0$ and $v_\phi = 0$. If $\Omega = \pi$, they are satisfied for $\theta = 0$, and $\theta = \pi$. Employing the 'zero-trace' stability condition of the linearized Landau-Lifshitz-Gilbert equation¹⁴, we find the critical current destabilizing the initial ($\theta = 0$) state in the form

$$I_{c, \text{DSV}}^0 = \frac{\alpha \mu_0 M_s d}{a_L^0 + a_R^0} \left(H_{\text{ext}} + H_{\text{ani}} + \frac{H_{dx} + H_{dy}}{2} - H_{dz} \right), \quad (9)$$

where a_L^0 and a_R^0 are calculated for $\theta \rightarrow 0$. Additionally, we have omitted here the terms resulting from τ_\perp because of their small contribution to the critical current. Equation (9) is analogous to the expression for critical current in SSV¹³. According to our calculations, the critical current in DSVs with F = Cobalt is 6-times smaller than in SSVs, as reported by Berger⁵. However, if F = Permalloy, the introduction of a second fixed magnetic layer reduces the critical current only by a factor of 2. This difference arises from the dependence of spin

accumulation on spin-flip length which is about 10-times longer in Cobalt than in Permalloy⁶.

To estimate the switching time in DSVs as well as in SSVs we employ the single-domain macrospin approximation to the central layer. Equations (1), including Eq. (3) and Eq. (4), completely describe the dynamics of central layer's spin, \hat{s} . In our simulations we assumed a constant current of density I . The positive current ($I > 0$) is defined for electrons flowing from F_R towards F_L (current then flows from F_L towards F_R); opposite current is negative. Apart from this, the demagnetization field of the free layer of elliptical cross-section with the axes' lengths 130 nm and 60 nm has been assumed, while external magnetic field was excluded, $H_{\text{ext}} = 0$. For each value of the current density, from Eq. (1) we found evolution of \hat{s} starting from an initial state until \hat{s} switched to the opposite state (provided such a switching was admitted). In all simulation, the spin was initially slightly tilted in the layer plane from the orientation $\hat{s} = (0, 0, 1)$, assuming $\theta_0 = 1^\circ$ and $\phi_0 = \pi/2$. A successful switching, with the switching time t_s , is counted when $\overline{s_z}(t_s) < -0.99$, where $\overline{s_z}(t)$ is the exponentially weighted moving average¹⁵, $\overline{s_z}(t) = \eta s_z(t) + (1 - \eta)\overline{s_z}(t - \Delta t)$, Δt is the integration step, and the weighting parameter $\eta = 0.1$. The moving average $\overline{s_z}$ is calculated only in time intervals, where $s_z(t)$ remains continuously below the value of -0.9 ; otherwise $\overline{s_z}(t) = s_z(t)$. Fig. 3 compares the switching times in DSVs and in the corresponding SSVs. In both cases shown in Fig. 3, a considerable reduction of the switching time is observed in DSVs. Similarly as for the critical current, the reduction of current required for switching in DSVs with Cobalt layers is larger from that in DSVs with Permalloy layers.

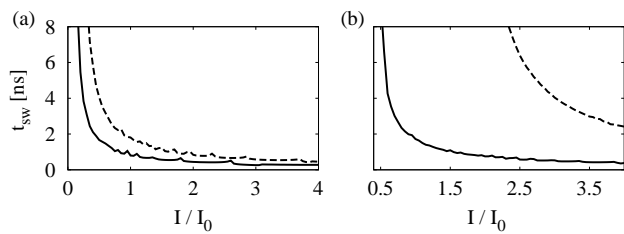


FIG. 3: Switching time in DSVs $F(20)/\text{Cu}(10)/F(8)/\text{Cu}(10)/F(20)$ in the antiparallel magnetic configuration, $\Omega = \pi$, (solid lines), and in SSVs $F(20)/\text{Cu}(10)/F(8)$ (dashed lines), where (a) F = Permalloy, (b) F = Cobalt. The switching time is shown as a function of the normalized current density I/I_0 , with $I_0 = 10^8 \text{ Acm}^{-2}$. The other parameters as in Fig.2.

IV. EXCHANGE-BIASED DSV

Let us consider now an asymmetric exchange-biased DSV structure with an antiferromagnetic layer IrMn adjacent to the F_R layer in order to pin its magnetic

moment in a required orientation, i.e. the structure $\text{Co}(20)/\text{Cu}(10)/\text{Py}(4)/\text{Cu}(4)/\text{Co}(10)/\text{IrMn}(8)$. The left magnetic layer, $F_L = \text{Co}(20)$, is assumed to be thick enough so its magnetic moment is fixed, $\hat{S}_L = \hat{e}_z$. In turn, magnetic moment of the right ferromagnetic layer, $F_R = \text{Co}(10)$, is fixed in the layer plane at a certain angle Ω with respect to \hat{S}_L due to the exchange-bias coupling to IrMn.

From Eqs. (6), (7), and (8) follows, that in a general case ($\Omega \neq 0$), the points $\theta = 0$ and $\theta = \pi$ are no more solutions of the conditions for fixed points, $v_\theta = 0$ and $v_\phi = 0$, because of the additional terms in STT, which appear in non-collinear situations (discussed in section II). These additional terms lead to a nontrivial θ -dependence of STT, and to a shift of the fixed points out of the collinear positions.

To analyze this effect in more details, let us consider first STT assuming \hat{s} in the layer plane ($\phi = \pi/2$). According to Eq. (7b) and Eq. (8b), and to the fact that the parameters b are much smaller than a , the component τ_ϕ is very small. In Fig. 4(a) we show the second component of the torque, namely τ_θ , as a function of the angle θ and for different values of the angle Ω . The configurations where $\tau_\theta = 0$ are presented by the contour in the base plane of Fig. 4(a).

In the whole range of the angle Ω , two 'trivial' zero points are present. Additionally, for small angles close to $\Omega = 0$, two additional zero points occur. The appearance of these additional zero points closely resembles non-standard wavy-like STT angular dependence, which has been already reported in single spin valves with magnetic layers made of different materials^{6,8,16}. Such a θ -dependence dictates that both zero-current fixed points ($\theta = 0, \pi$) become simultaneously stabilized (destabilized) for positive (negative) current. This behavior is of special importance for stabilization of the collinear configurations, and for microwave generation driven by current only (without external magnetic field)^{6,8,17}. We note, that in contrast to SSVs, the wavy-like θ -dependence in exchange-biased DSVs is related rather to asymmetric geometry of the multilayer than to bulk and interface spin asymmetries. This trend is depicted in Fig. 4(b), where we show variation of STT for different thicknesses of F_R at $\Omega = 0$. The wavy-like torque angular dependence appears for the thickness of F_R markedly different from that of F_L .

Making use of the above described STT calculations, extended to arbitrary orientation of \hat{s} , we performed numerical simulations of spin dynamics induced by a constant current in zero external magnetic field ($H_{\text{ext}} = 0$). The sample cross-section was assumed in the form of an ellipse with the axes' lengths 130 nm and 60 nm. As before, the numerical analysis has been performed within the macrospin framework, integrating equation of motion, Eq.(1). In the simulation we analyzed the long-term current-induced spin dynamics started from the initial state corresponding to $\theta_0 = 1^\circ$, $\phi_0 = \pi/2$.

As one might expect, the current-induced spin dynam-

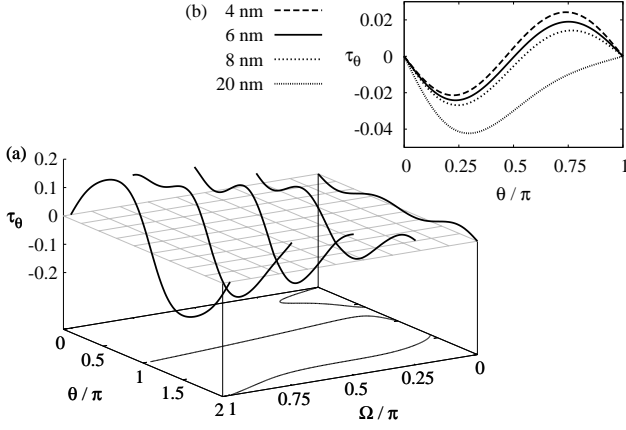


FIG. 4: (a) STT acting on the central magnetic layer in $\text{Co}(20)/\text{Cu}(10)/\text{Py}(4)/\text{Cu}(4)/\text{Co}(10)/\text{IrMn}(8)$ exchange-biased DSV as a function of the angle θ , calculated for $\Omega = k\pi/4$, $k = 0, 1, 2, 3, 4$. The contour plot in the base plane corresponds to zeros of τ_θ . (b) Wavy-like STT angular dependence in exchange biased DSV for $\Omega = 0$, calculated for different thicknesses of the F_R layer. STT is shown in the units of $\hbar|I|/|e|$. The other parameters as in Fig.2.

ics of the free layer depends on the angle Ω , current density I , and on current direction. To designate different regimes of STT-induced spin dynamics, we constructed a dynamical phase diagram as a function of current and the angle Ω . The diagram shows the average value $\langle s_z \rangle$ of the z component of the free layer net-spin in a stable dynamical regime (see Fig. 5a), as well as its dispersion $D(s_z) = \sqrt{\langle s_z^2 \rangle - \langle s_z \rangle^2}$ (see Fig. 5b). The average value $\langle s_z \rangle$ provides an information on the spin orientation, whereas the dispersion distinguishes between static states (for which $D = 0$) and steady precessional regimes (where $D > 0$), in which the z component is involved. For each point in the diagram, a separate run from the initial biased state $\phi_0 = \pi/2$ and $\theta_0 = 1^\circ$ was performed. In the $\langle s_z \rangle$ diagram, Fig. 5(a), one can distinguish three specific regions. Region (i) covers parameters for which a weak dynamics is induced only: \hat{s} finishes in the equilibrium stable point which is very close to $\hat{s} = (0, 0, 1)$. As the angle Ω increases, STT becomes strong enough to cause switching, as observed in the region (ii). The higher the angle Ω , the smaller is the critical current needed for destabilization of the initial state. For smaller Ω , the current-induced dynamics occurs for currents flowing in the opposite direction, see the region (iii). This behavior is caused by different sign of STT in the initial state. From $\langle s_z \rangle$ we conclude, that neither of the previously mentioned stable states is reached. To elucidate the dynamics in region (iii), we constructed the corresponding map of $D(s_z)$, Fig. 5(b). This map reveals three different modes of current-induced dynamics. For small current amplitudes, in-plane precession (IPP) around the initial stable position is observed. The precessional angle rises

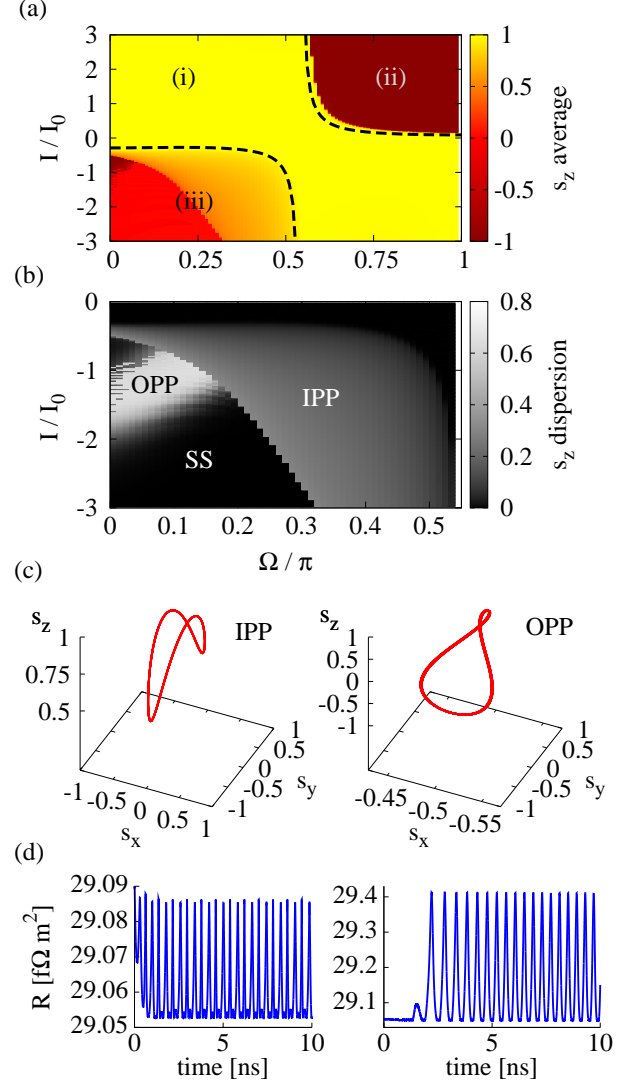


FIG. 5: (Color online) Dynamical phase diagram for $\text{Co}(20)/\text{Cu}(10)/\text{Py}(4)/\text{Cu}(4)/\text{Co}(10)/\text{IrMn}(8)$ exchange-biased double spin valve as a function of the angle Ω and normalized current density I/I_0 (with $I_0 = 10^8 \text{Acm}^{-2}$): (a) average value of the s_z spin component; (b) dispersion of the s_z spin component; (c) typical precessional orbits; (d) resistance oscillations associated with the IPP for $\Omega = 0.4\pi$ and $I = -1.3I_0$ (left part), and with the OPP for $\Omega = 0.1\pi$ and $I = -1.3I_0$ (right part). The other parameters as in Fig.3.

with increasing current amplitude. Above a certain critical value of I , the precessions turn to out-of-plane precessions (OPPs). In a certain range of Ω , the OPPs collapse to a static state (SS), where the spin \hat{s} remains in an out-of-plane position close to $\pm \hat{e}_x$.

As \hat{S}_R departs from the collinear orientation, the critical current needed for destabilization of the initial state increases. This growth is mostly pronounced close to $\Omega = \pi/2$. To describe the critical current, we analyzed Eq. (5) with respect to the stability of \hat{s} in the upper po-

sition. Assuming that even in noncollinear configuration the stable position of \hat{s} is close to $\theta = 0$, we have linearized Eq. (5) around this point for arbitrary Ω . Then, for the critical current needed for destabilization of the considered stable state we find

$$I_{c, \text{EBDSV}}^0 \simeq \frac{\alpha \mu_0 M_s d \left(H_{\text{ani}} + \frac{H_{dx} + H_{dy}}{2} - H_{dz} \right)}{a_L^0(\Omega) - a_R^0(\Omega) \cos \Omega}, \quad (10)$$

where $a_L^0(\Omega)$ and $a_R^0(\Omega)$ are calculated (for each configuration) assuming $\theta \rightarrow 0$. Comparison of Eq. (10) with the results of numerical simulations is shown in Fig. 5. When considering the opposite stable point as the initial state, we need to take a_L and a_R for $\theta \rightarrow \pi$. Clearly, to destabilize the $\theta = \pi$ state one needs current of opposite direction.

Current-induced oscillations are usually observed experimentally *via* the magnetoresistance effect³. When electric current is constant, then magnetic oscillations cause the corresponding resistance oscillations, which in turn lead to voltage oscillations. The later are measured directly in experiments. In Fig. 5(d) we show oscillations in the system resistance associated with the IPP (left) and OPP (right). As the amplitude of the oscillations corresponding to the OPP mode is sufficiently large to be measured experimentally, the amplitude associated with the IPP mode is relatively small. This is the reason, why IPP mode is usually not seen in experiments.

V. DISCUSSION AND CONCLUSIONS

We have calculated STT in metallic dual spin valves for arbitrary magnetic configuration of the system, but with magnetic moments of the outer magnetic films fixed in their planes either by large coercive fields or by exchange anisotropy. In the case of symmetric DSV structures, we found a considerable enhancement of STT in the antiparallel magnetic configuration. This torque enhancement leads to reduction of the critical current for switching as well as to reduction of the switching time. The switch-

ing improvement has been found to be dependent on the spin-flip lengths in the magnetic and nonmagnetic layers. According to our numerical simulations, an ultrafast subnanosecond current-induced switching processes can occur in DSVs with antiparallel magnetic moments of the outermost magnetic films.

In exchange-biased spin valves we have identified conditions which can lead to various types of spin dynamics. For $\Omega \lesssim \pi/2$, the negative current excites the central magnetic layer, while for $\Omega \gtrsim \pi/2$, opposite current direction is needed. We have evaluated parameters for which switching to a new stable state or to a precessional regime appears. This is especially interesting from the application point of view. However, the static state (SS) should be treated carefully. Such a state is often connected with the *wavy*-like angular dependence of STT^{13,16,17}. The SS becomes stable in the framework of macrospin model, when STT disappears in a certain noncollinear configuration. However, experimentally such a state has not been observed so far¹⁶. It has been shown in more realistic micromagnetic approach, that this static state may correspond to out-of-plane precessions¹⁸. The reason of this is the finite strength of exchange coupling in magnetic film, which does not fully comply with the macrospin approximation in some cases.

Finally, we have derived an approximate formula for the critical current in exchange biased DSVs, valid for non-collinear magnetic configurations. This formula, Eq.(10), is in good agreement with the numerical simulations.

Acknowledgment

The work has been supported by the the EU through the Marie Curie Training network SPIN-SWITCH (MRTN-CT-2006-035327). M.G. also acknowledges support VEGA under Grant No. 1/0128/08, and J.B. acknowledges support from the Ministry of Science and Higher Education as a research project in years 2006-2009.

* Electronic address: balaz@amu.edu.pl

¹ J. C. Slonczewski, J. Magn. Magn. Mater. **159**, L1 (1996).

² L. Berger, Phys. Rev. B **54**, 9353 (1996).

³ S. I. Kiselev, J. C. Sankey, I. N. Krivorotov, N. C. Emley, R. J. Schoelkopf, R. A. Buhrman, and D. C. Ralph, Nature **425**, 380 (2003).

⁴ J. A. Katine, F. J. Albert, R. A. Buhrman, E. B. Myers, and D. C. Ralph, Phys. Rev. Lett. **84**, 3149 (2000).

⁵ L. Berger, J. Appl. Phys. **93**, 7693 (2003).

⁶ J. Barnaś, A. Fert, M. Gmitra, I. Weymann, and V. K. Dugaev, Phys. Rev. B **72**, 024426 (2005).

⁷ T. Valet and A. Fert, Phys. Rev. B **48**, 7099 (1993).

⁸ M. Gmitra and J. Barnaś, Phys. Rev. Lett. **96**, 207205 (2006).

⁹ A. A. Kovalev, A. Brataas, and G. E. W. Bauer, Phys. Rev. B **66**, 224424 (2002).

¹⁰ O. Boulle, V. Cros, J. Grollier, L. G. Pereira, C. Deranlot, F. Petroff, G. Faini, J. Barnaś, and A. Fert, Nature Phys. **3**, 492 (2007).

¹¹ M. D. Stiles and A. Zangwill, Phys. Rev. B **66**, 014407 (2002).

¹² K. Xia, P. J. Kelly, G. E. W. Bauer, A. Brataas, and I. Turek, Phys. Rev. B **65**, 220401(R) (2002).

¹³ M. Gmitra and J. Barnaś, Appl. Phys. Lett. **89**, 223121 (2006).

¹⁴ S. Wiggins, *Introduction to Applied Nonlinear dynamical Systems and Chaos* (Springer-Verlag, 1990).

¹⁵ S. W. Roberts, Technometrics **42**, 97 (2000).

- ¹⁶ O. Boule, V. Cros, J. Grollier, L. G. Pereira, C. Deranlot, F. Petroff, G. Faini, J. Barnaś, and A. Fert, Phys. Rev. B **77**, 174403 (2008).
- ¹⁷ P. Balaz, M. Gmitra, and J. Barnaś, Phys. Rev. B **79**, 144301 (2009).
- ¹⁸ E. Jaromirska, P. Baláž, L. López Díaz, J. Barnaś, to be published.